Cell Reports
Physical Science

CellPress
OPEN ACCESS

Article

Thin layer lightweight and ultrawhite hexagonal boron nitride nanoporous paints for daytime radiative cooling

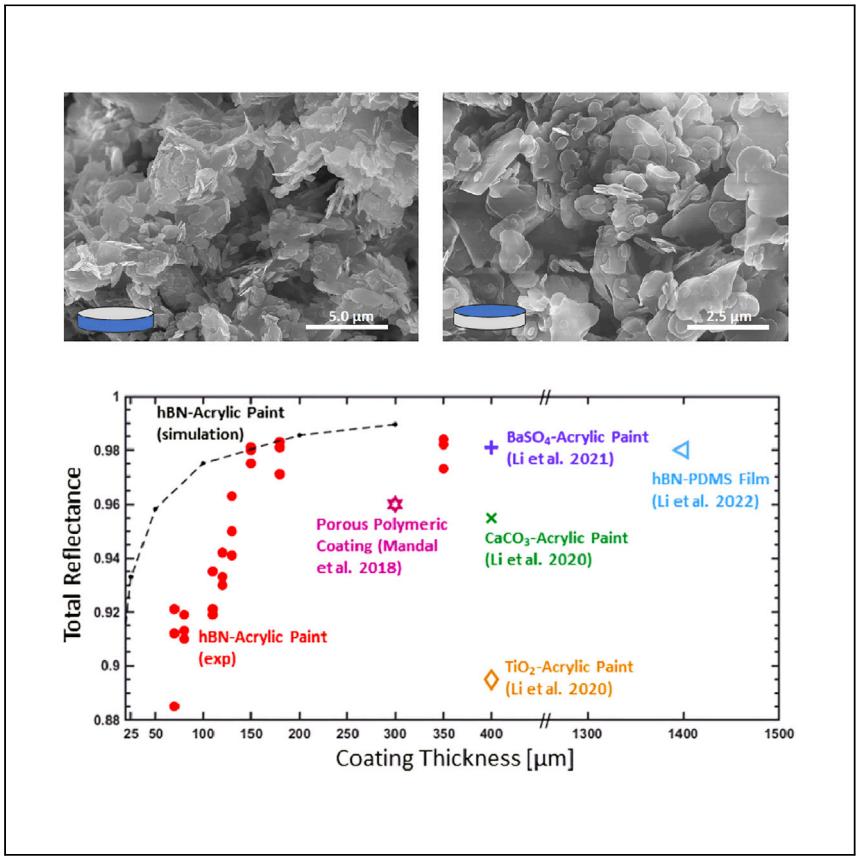

Thin and lightweight radiative cooling paints are needed for many weight-sensitive applications. The ultrawhite hBN-acrylic paint created in this work shows a high solar reflectance of 97.9% and full daytime cooling with a paint layer of only 150 µm thick, demonstrating significant reduction in thickness and weight.

Andrea Felicelli, Ioanna Katsamba, Fernando Barrios, ..., Joseph Peoples, George Chiu, Xiulin Ruan

gchiu@purdue.edu (G.C.)
ruan@purdue.edu (X.R.)

Highlights

Ultrawhite cooling paint is created incorporating hBN nanoplatelets and nanopores

High solar reflectance of 97.9% is achieved with 150-µm thin and lightweight layer

Full daytime cooling under direct sunlight with 5°–6°C below ambient on average

Simulations reveal high scattering coefficient and strong backscattering

Felicelli et al., Cell Reports Physical Science 3, 101058
October 19, 2022
https://doi.org/10.1016/j.xcrp.2022.101058

Please cite this article in press as: Felicelli et al., Thin layer lightweight and ultrawhite hexagonal boron nitride nanoporous paints for daytime radiative cooling, Cell Reports Physical Science (2022), https://doi.org/10.1016/j.xcrp.2022.101058

Cell Reports
Physical Science

Article

Thin layer lightweight and ultrawhite hexagonal boron nitride nanoporous paints for daytime radiative cooling

Andrea Felicelli,[1,2] Ioanna Katsamba,[1,2] Fernando Barrios,[1] Yun Zhang,[1] Ziqi Guo,[1] Joseph Peoples,[1] George Chiu,[1,*] and Xiulin Ruan[1,3,*]

SUMMARY

Thin and lightweight radiative cooling paints are needed for many weight-sensitive applications. However, it is difficult to achieve high solar reflectance with thin layers. This work develops ultrawhite hBN-acrylic paints that achieve solar reflectance of 97.9% and sky window emissivity of 0.83 with only 150 μm thickness and 0.029 g/cm^2 weight, representing significant reductions from previous radiative cooling paints. The high refractive index and nanoplatelet morphology of hBN enable a unique combination of Mie scattering-like high scattering coefficient and Rayleigh scattering-like strong backscattering, and a porosity of 44.3% offers high refractive index contrast between hBN and air; all contribute to achieve high solar reflectance with a thin coating. Field tests show full daytime cooling under direct sunlight, reaching 5–6°C below ambient temperature on average during daylight hours. Our hBN-acrylic paint demonstrates comparable cooling performance with recent best technologies, and the thinness and light weight reduce barriers toward many practical applications.

INTRODUCTION

According to the U.S. Department of Energy, 6% of the average household's energy use goes toward space cooling.[1] This is due to cooling technologies that rely on electricity generated via processes with high carbon emissions. At a time when many are interested in working to address climate crisis affecting our planet, it is vital to look into ways to reduce our carbon footprint in everyday life. Radiative cooling is a passive cooling technology that accomplishes this by reflecting solar irradiation and emitting thermal radiation via an atmospheric transparent window (a wavelength range of 8–13 μm) into deep space, therefore not relying on electricity generation.[2] When a material emits more heat in the sky window than it absorbs from the solar irradiation, the resulting net cooling power allows cooling the surface on earth to a temperature below the surrounding ambient. Conventional air conditioning removes heat from buildings into the ambient air,[3] so heat still stays in the city and on the earth. Radiative cooling, on the other hand, directly loses heat to the deep space, reducing the heat island effect and cooling down the earth.

Radiative cooling coating and composite technologies have greatly advanced throughout the years. In one of the earliest studies on paints for radiative cooling, a thin commercial titanium oxide-based paint layer was coated on an aluminum plate to achieve daytime radiative cooling.[4] However, the high solar reflectance was mostly from the metal substrate and not the paint itself (i.e., no substrate

[1]School of Mechanical Engineering and Birck Nanotechnology Center, Purdue University, West Lafayette, IN, USA

[2]These authors contributed equally

[3]Lead contact

*Correspondence: gchiu@purdue.edu (G.C.), ruan@purdue.edu (X.R.)

https://doi.org/10.1016/j.xcrp.2022.101058

Please cite this article in press as: Felicelli et al., Thin layer lightweight and ultrawhite hexagonal boron nitride nanoporous paints for daytime radiative cooling, Cell Reports Physical Science (2022), https://doi.org/10.1016/j.xcrp.2022.101058

independence was demonstrated). Another study measured the radiative cooling performance of several commercially available white paints.[5] There have also been heat reflecting paints developed reaching 91% reflectance.[6] These early studies on paints showed the need for improved solar reflectance in paints in order to reach full daytime cooling.

Some other approaches to radiative cooling have involved non-paintable technologies. Outside of explicit radiative cooling considerations, sintered reflective ceramic coatings consisting of Al_2O_3, hBN, and other particles were pursued for space applications and achieved spectral reflectance of 87.5%.[7] In the past decade, full daytime radiative cooling has been achieved in photonic materials, such as integrated photonics solar reflectors and thermal emitters with several layers of silicon oxide and hafnium oxide,[8] polymer coated, fused silica mirrors,[9] resonant polar dielectric microspheres embedded in a polymer matrix with a metallic bilayer,[10] structural materials consisting of delignified and densified wood,[11] pressed nanocomposite films embedded with hBN,[12,13] with the latter achieving 98% solar reflectance at a rather thick film of 1.4 mm,[13] and other photonic and multilayer structures.[14] However, these approaches have one or more limitations such as complicated multi-layered structures, a metallic layer, or large thickness of more than 1 mm to achieve the needed solar reflectance. Meanwhile, although radiative cooling films often have end components of particles and polymers, which are similar to that of paints, they are not paintable technologies hence limiting their applications. In this scenario, radiative cooling film technologies and paint technologies should not be mixed, because a film technology usually cannot transit to a paint technology, or at least involve significant barriers to be resolved. Cooling paints, defined as being applicable using standard brush, roller, or spray-painting techniques, are desired to allow ease of use and viable applications on non-flat surfaces, compared with films.

For this reason, there is a renaissance of radiative cooling paint technology recently. A double-layer acrylic coating embedded with titanium dioxide and carbon black nanoparticles was predicted to achieve full daytime cooling.[15] Silica microsphere media without a binder were tested to show partial daytime cooling,[16] and paint-like porous polymeric coatings with 5.5 μm and 200 nm pore sizes were developed with full daytime cooling.[17] Furthermore, a strategy of broad particle size distribution was proposed to enhance the solar reflectance than a single size.[18] Recently, high-concentration $CaCO_3$- and $BaSO_4$-based paints have been developed with high solar reflectance and sky window emittance, that can achieve full daytime radiative cooling capabilities.[19–21] $BaSO_4$ has high band gaps of 7.27 eV that can eliminate the UV absorption, and the high concentration and broad particle size distribution enable broadband high solar reflectance. It was also suggested that the average particle size should be in the neighborhood of the peak solar wavelength (500 nm), and these sizes are more effective in scattering the sunlight than particle or pore size that is either too small (<100 nm) or too large (>1 μm).[15,18–21] Although high performance and greater ease of use have been demonstrated with paint technologies like these, they required 300 μm thickness to reach 96% solar reflectance in the porous polymer coatings[17] and 400 μm thickness to reach the highest reported solar reflectance of 98.1% in $BaSO_4$ paint, the whitest paint reported to date.[21] Other ultrawhite paints may need mm thickness to reach optimal performance.[22] In contrast, typical commercial paint thickness is 120 μm on vehicles and 150–200 μm on buildings, and each coat by brush or roller adds 50–75 μm of paint when dried. The much larger thickness of current radiative cooling paints would mean 5–8 coats and much more labor. Moreover, the density of BaSO4 (4.5 g/cm^3) is higher than the commercial TiO_2 (4.23 g/cm^3). Therefore, the best radiative cooing paints represent

significantly higher thickness and weight than commercial paints currently in use, and perhaps too high for many important applications that are weight sensitive, such as automobiles, wearables, aerospace, and space applications. Considering these barriers, there remains an urgent need to develop high-performance yet significantly thinner and/or lighter radiative cooling paints. This is a very challenging task, as it means that the backscattering coefficient needs to be remarkably enhanced compared with the state of the art.

In this work, we have designed and fabricated thin and light-weight hBN-acrylic nanoporous paints, on which we have experimentally demonstrated the high solar reflectance, sky window emissivity, and full daytime subambient cooling. A provisional patent based on this work was filed with the U.S. Patent and Trademark Office (USPTO) on August 28, 2021, with application number 63238124. The hBN in a nanoplatelet form was chosen because of its appropriate band gap and unique morphology. The upper bound of the photon energy in the solar spectrum is 4.13 eV, hence the material band gap needs to be higher than 4.13 eV to eliminate solar absorption. However, as the band gap increases, the refractive index decreases which weakens scattering and reflection. Therefore, a band gap moderately higher than 4.13 eV is preferred.[23] hBN has band gap of 5.96 eV, which is above 4.13 eV but significantly lower than that of $BaSO_4$, resulting in a refractive index of 2.1–2.3 in the solar spectrum when BN planes are oriented parallel to the electric field (hereafter called "in-plane" orientation, or perpendicular to the incident wave) and 1.4–1.6 when BN planes are vertical to the electric field (or parallel to the incident wave).[24,25] In contrast, the refractive index is only 1.66 for $BaSO_4$.[23] Our simulations also show that the higher refractive index and nanoplatelet morphology for hBN yield an unusual combination of Mie scattering-like high scattering coefficient and Rayleigh scattering-like strong backscattering, both of which favor high solar reflectance. Furthermore, the nanoplatelets used had a diameter of 332 ± 193 nm, where the average diameter is optimum to strongly scatter the solar spectrum and the non-uniform diameter distribution enables efficient broadband scattering compared with a single size.[18,26] A high nanoplatelet loading of 60% volume concentration (hereafter it means the volume concentration among the solid phases in the wet paint phase if not otherwise stated; after the paint is dried, the layer develops a porosity of 0.443, hence the volume concentrations of hBN, acrylic, and air become 33.4%, 22.3%, and 44.3% respectively) is used to maximize light scattering while maintaining the desirable mechanical properties of the polymer binder. With this concentration, we achieved 97.9% reflectance in the solar spectrum and a sky window emissivity of 0.83 from a dried paint layer with a thickness of only 150 μm and weight of only 0.029 g/cm^2. Outdoor testing showed an average of 5°C–6°C cooling below ambient temperature on the sample's surface. The thickness and weight are significantly lower than previous records of radiative cooling paints, while maintaining a solar reflectance among the highest. The thickness is now reduced to the typical range of commercial paints, and the light weight is attractive for weight-sensitive applications, such as automobiles, wearables, aerospace and space applications. Furthermore, it has wear-resistance, viscosity, and water resistance consistent with that of industry standards at only a fraction of the layer thickness.

RESULTS AND DISCUSSION

Paint fabrication and characterizations

First, we have designed and fabricated hBN-acrylic coatings with a range of different thicknesses. Because a high concentration is desirable to promote effective light scattering within the material, the paint was loaded with hBN nanoplatelets at

Please cite this article in press as: Felicelli et al., Thin layer lightweight and ultrawhite hexagonal boron nitride nanoporous paints for daytime radiative cooling, Cell Reports Physical Science (2022), https://doi.org/10.1016/j.xcrp.2022.101058

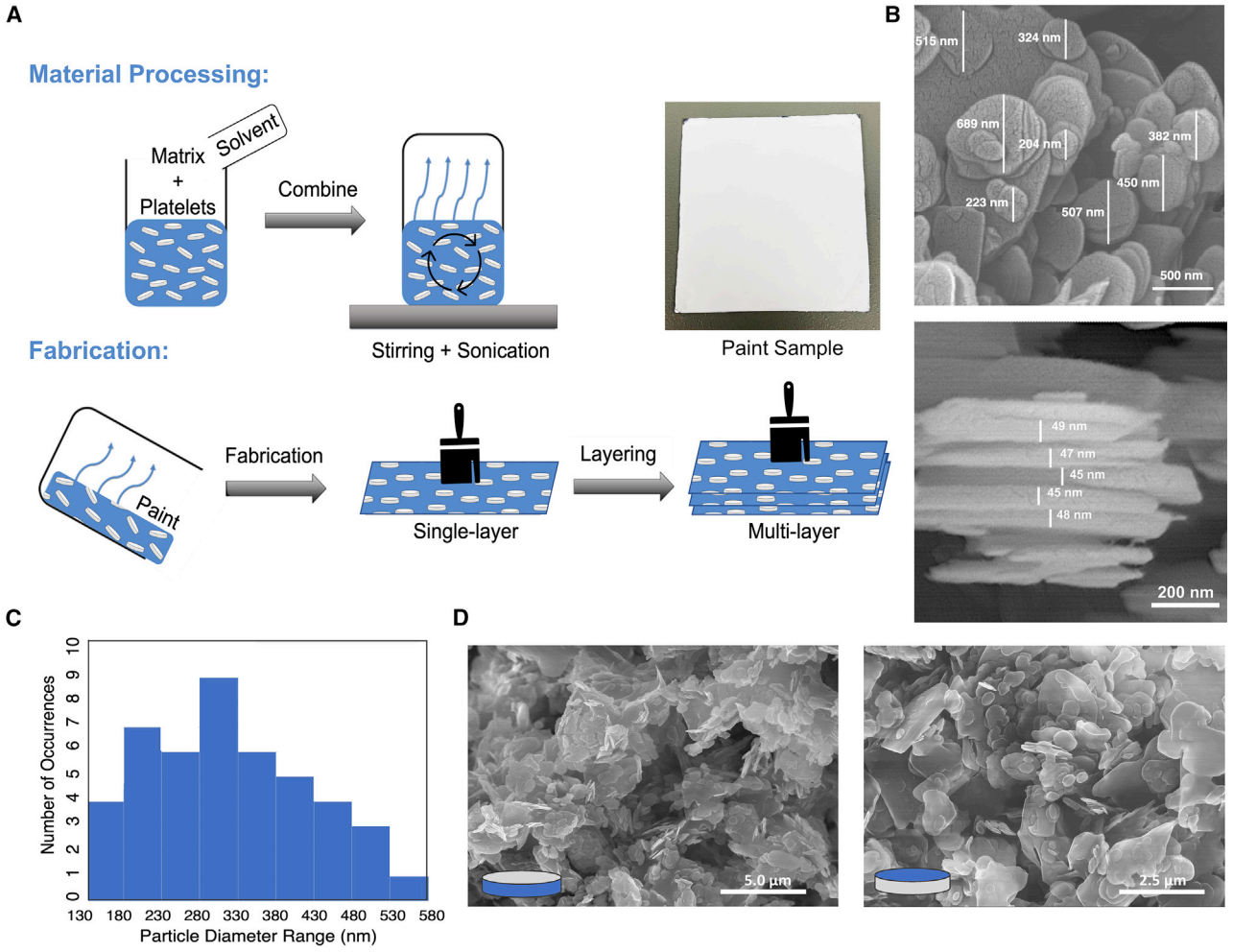

Figure 1. Radiative cooling paint preparation and characterizations

(A) Schematic of the hBN-acrylic paint making process and an example image of a painted sample.

(B) Top and side view SEM images of the hBN nanoplatelets. The nanoplatelet diameter and thickness distributions were determined to be 332 ± 193 and 45 ± 3 nm, respectively.

(C) Particle diameter distribution of 50 particles demonstrated in a histogram, with the largest proportion of the diameters measured shown to be between 280 and 330 nm.

(D) SEM images of hBN-acrylic nanocomposite coating, with top-down view and cross-section view.

hBN: acrylic = 60:40 volume ratio. Samples were prepared by pouring or brushing uniform layers onto flat glass or aluminum substrates and allowed to fully dry in a fume hood. The resulting samples are visibly ultrawhite and opaque, with consistent layer thickness distributions across the substrates. Figure 1A illustrates the techniques used in this research, as well as an example of the paint layer tested throughout.

Scanning electron microscopy (SEM) imaging was used to determine nanoplatelet morphology, orientation, and observe their dispersion throughout the acrylic matrix. The nanoplatelet structure of the hBN has a high aspect ratio and directional properties, as well as a high degree of variability in diameter and low variability in thickness (Figure 1B). An overall diameter distribution of 332 ± 193 nm (Figure 1C) and a fairly uniform distribution of platelet thickness of 45 ± 3 nm (Figure 1B) are observed, which should contribute to improved light scattering and higher solar

Please cite this article in press as: Felicelli et al., Thin layer lightweight and ultrawhite hexagonal boron nitride nanoporous paints for daytime radiative cooling, Cell Reports Physical Science (2022), https://doi.org/10.1016/j.xcrp.2022.101058

reflectance values as a result. This is due to an average size in the neighborhood of the solar peak wavelength and a broad size distribution.[26] The acrylic matrix that encapsulates and bonds the nanoplatelet filler gives the material improved reliability under various conditions because of the polymer-filler composition, similar to the majority of commercially available paints, although with a higher pigment loading (Figure 1D). The platelets can be observed to be in various orientations. Some horizontal orientation may be achieved because of the shear force effects of pouring techniques, where the paint is allowed to flow vertically downwards along the substrate because of gravitational effects, or brushing/screen-printing techniques, where the equipment distributes the paint directionally along the substrate surface. This orientation, with the surface of the platelet perpendicular to incident sunlight, allows the larger refractive index of the hBN to take effect and enable efficient scattering.[24] Although there remain some particles that can be observed to be at a more angled orientation (Figure 1D), high radiative cooling performance is still achieved. This suggests desired performance can be achieved without perfect particle alignment. DMF is added to the mixture at a 1:6 volume ratio, which was found to reduce viscosity associated with the high concentration of nanoplatelets to a usable level while maintaining low evaporation time of 2–4 h depending on coating thickness. The average porosity of a dried paint layer is calculated to be 44.3%, with an SD of 1.4%. The pores can facilitate strong scattering and reduce the paint layer thickness needed, as they enable hBN-air interfaces with high refractive index contrast (n_{hBN}/n_{air} = 2.3:1). In contrast, porous polymers[17] or fully dense hBN-PDMS photonic films without voids[13] do not have such high contrast. It should be noted that the volume concentrations of hBN and acrylic are 60% and 40% among the solid phases in the wet paint state; after the paint is dried with a porosity of 44.3%, the volume concentrations of hBN, acrylic, and air become 33.4%, 22.3%, and 44.3% respectively. Although it is acknowledged that the porosity can lead to soiling of the material over time in application, it is recommended that a hydrophobic, self-cleaning topcoat is used. The use of topcoats is a well-established technique and is already very frequently used to address this issue for commercial paints in outdoor applications. Alternatively, binders that show strong hydrophobic properties can also be promising. Details on the porosity calculation can be found in Experimental procedures.

Optical property characterization and modeling

Radiative cooling performance including daytime subambient cooling is optimized in materials by achieving high reflectance in the solar spectrum of 250–2,500 nm and a high emittance in the sky window of 8–13 μm. In coatings and paints, this can be done by designing the material on the basis of the properties of the nanoparticle filler and matrix. The acrylic matrix not only helps provide ease of use and improved reliability in application but also contributes to the high sky window emissivity. The hBN-acrylic coatings showed excellent solar reflectance at various layer thicknesses. At 150 μm, the coating's solar reflectance begins to saturate at 97.9%, and the emissivity is measured to be 0.83 (Figure 2A). At 70 μm, the solar reflectance is still 90.9%, and the sky window emissivity is 0.78 (Figure 2B). Figure 2C shows the solar reflectance measured as a function of thicknesses, including 91.6%, 92.1%, 93.0%, 95.0%, and 98.2% for 80-, 110-, 120-, 130-, and 350-μm-thick coatings, respectively. Saturation of reflectance at higher coating thickness, as seen in Figure 2C, demonstrates that for maximum solar reflectance, the coating does not need to be thicker than 150 μm. Figure 2C also shows that at 150 μm thickness, our hBN-acrylic nanoporous paint achieves comparable or higher solar reflectance than previous best radiative cooling paints, films, and porous polymers,[13,17,19–21] but the thickness is reduced by 50% or more. Furthermore, the density of hBN is only 2.1 g/cm^3, which is less than half of $BaSO_4$ at 4.5 g/cm^3. Hence the weight of the hBN-acrylic coating is

Please cite this article in press as: Felicelli et al., Thin layer lightweight and ultrawhite hexagonal boron nitride nanoporous paints for daytime radiative cooling, Cell Reports Physical Science (2022), https://doi.org/10.1016/j.xcrp.2022.101058

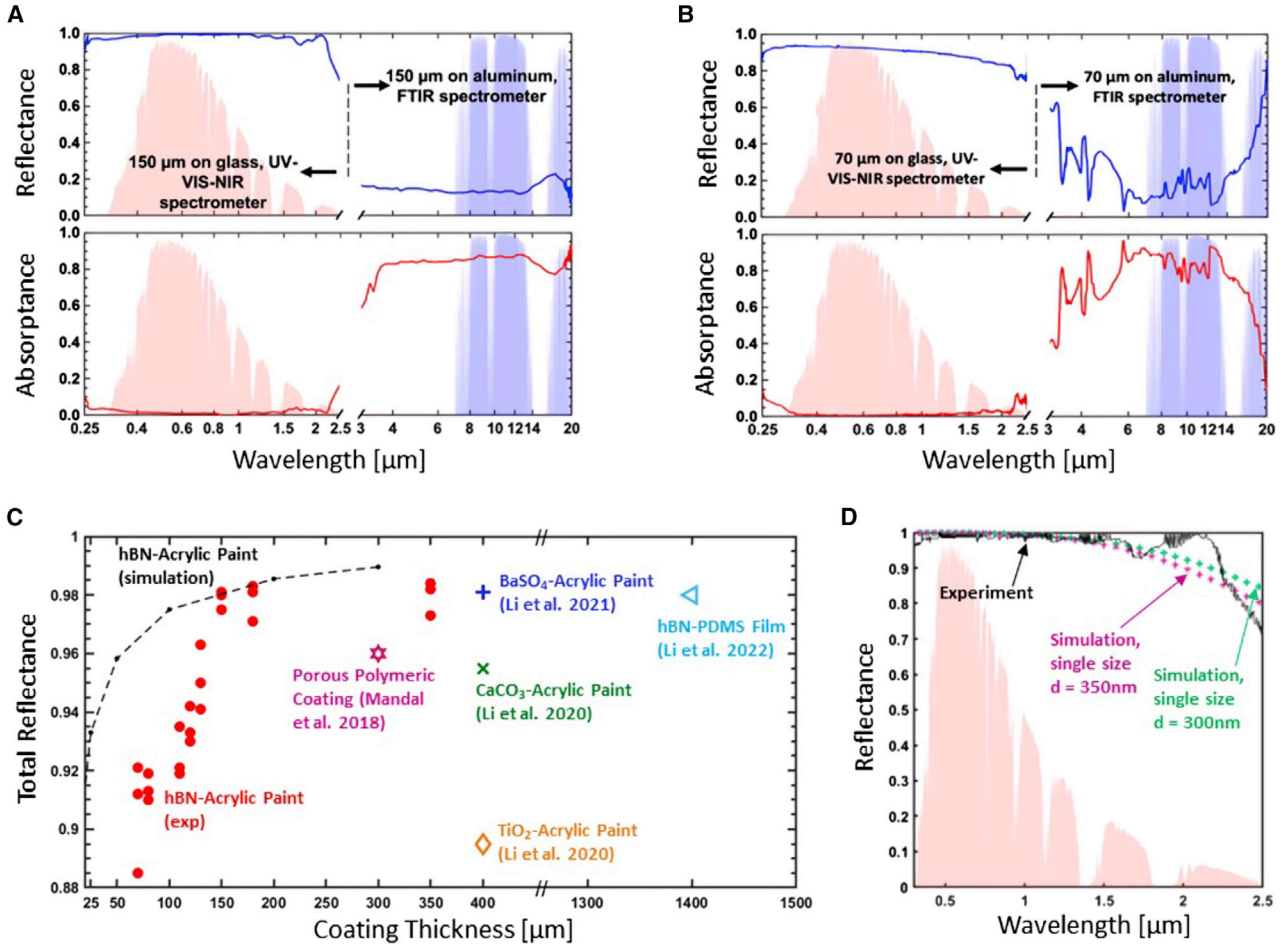

Figure 2. Spectral characterization results for hBN-acrylic coatings of different thicknesses with various substrates and simulation results

(A) Spectral characterization of a 150-μm-thick layer of hBN-acrylic coating. The total solar reflectance is 97.9% and the total sky window emissivity is 0.83. Measurements from 0.25–2.5 μm were performed with a 1-mm-thick glass substrate to avoid reflectance from the substrate, and measurements from 3.0–20 μm were performed with a 1-mm-thick aluminum substrate to avoid emissivity contribution from the substrate.

(B) Spectral characterization of a 70-μm-thick layer of hBN-acrylic coating. The total solar reflectance is 90.9% and the total sky window emissivity is 0.78.

(C) The total solar reflectance as a function of the coating thicknesses. All hBN-acrylic paint samples (red dots) were measured on 1-mm-thick glass substrates. The simulated total reflectance (dashed line) as a function of the nanocomposite's thickness is calculated via the Monte Carlo method. Previous literature data are also provided here and given in Table 1.

(D) Solar reflectance of hBN-acrylic, the simulation results agree well with the experiments. Two different single sizes were used, diameters of 300 and 350 nm.

much reduced from previous cooling paints (a detailed compassion is given later in the paper). Moreover, at 350 μm, 50 μm less than the 400 μm thickness required to reach 98.1% in previous work,[21] we measured 98.2% solar reflectance. Our measured solar reflectance values are also significantly higher than commercial heat-reflective paints.[6] Figure 2D shows a comparison between the experimental solar reflectance with Monte Carlo simulation data, which is described in detail subsequently.

To explain the ultra-high solar reflectance achieved for such a thin paint layer, the scattering coefficient and asymmetry parameter are calculated for hBN nanoplatelets using COMSOL, and the results are compared with those for $BaSO_4$ spherical nanoparticles in Figures 3A and 3B. The refractive indices are given in Figure S1 and the validation of the COMSOL model against the Mie theory is shown in Figure S2 in

Please cite this article in press as: Felicelli et al., Thin layer lightweight and ultrawhite hexagonal boron nitride nanoporous paints for daytime radiative cooling, Cell Reports Physical Science (2022), https://doi.org/10.1016/j.xcrp.2022.101058

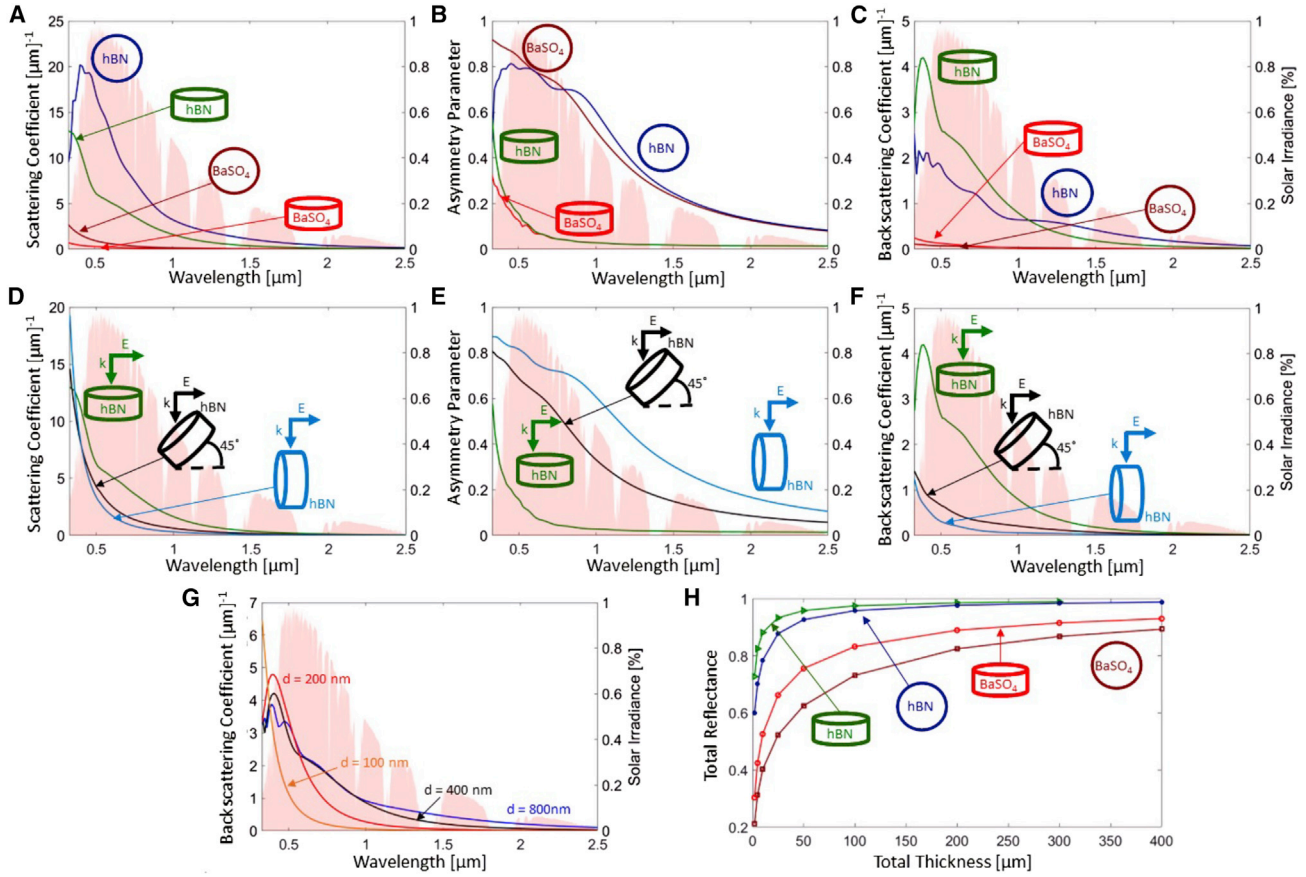

Figure 3. Simulations of the optical properties of various particles and the total reflectance of nanocomposites

(A) Scattering coefficient of four different particles, with different morphology and refractive index: the spherical $BaSO_4$ (brown), the platelet hBN (green), the platelet $BaSO_4$ (red), and the spherical hBN (blue). The refractive indices of $BaSO_4$ and hBN are given in Figure S1.

(B) Asymmetry parameter of the four particles.

(C) The backscattering coefficient of the four particles.

(D) The scattering coefficient of the platelet hBN with varying orientations, in-plane (green), 45° (black), and cross-plane (light blue).

(E) The asymmetry parameter of the platelet hBN with varying orientations.

(F) The backscattering coefficient of the platelet hBN with varying orientations.

(G) The backscattering coefficient of the hBN with different diameters of 100, 200, 400, and 800 nm.

(H) The predicted total reflectance as a function of the total coating thickness of the four different particles: the spherical $BaSO_4$ (brown) and the platelet hBN (green), as well as the two imaginary particles, the platelet $BaSO_4$ (red) and the spherical hBN (blue).

the supplementary material. Both nanoparticles have the same diameter of 370 nm, whereas the thickness of the platelets is 50 nm. Figure S3 shows the simulation setup for the scattering coefficient in COMSOL and the solar reflectance with Monte Carlo simulations. It is very interesting to note that hBN nanoplatelets show higher scattering coefficient (Figure 3A) and lower asymmetry parameter (i.e., more backscattering) (Figures 3B and 3C) in the in-plane direction in the entire spectrum than spherical $BaSO_4$, the previous state of the art. This result is significant and surprising. The asymmetry parameter gives important insights related to the form of scattering. It is close to unity when the backscattering is very narrow; this is known as geometric scattering. In contrast, the asymmetry parameter is close to zero when Rayleigh scattering occurs. For spherical particles, Mie scattering is usually favorable for achieving high reflectance because it provides a high scattering coefficient. However, a drawback is in the weaker backscattering. On the other hand, Rayleigh scattering offers equal backward and forward scattering; however the scattering coefficient is too small. A natural

Please cite this article in press as: Felicelli et al., Thin layer lightweight and ultrawhite hexagonal boron nitride nanoporous paints for daytime radiative cooling, Cell Reports Physical Science (2022), https://doi.org/10.1016/j.xcrp.2022.101058

question is whether the high, Mie scattering-like scattering coefficient and the strong, Rayleigh scattering-like backscattering can be achieved simultaneously. Clearly it is not feasible with spherical particles. However, this is achieved with the proposed hBN nanoplatelets. Further comparison between the asymmetry parameter of platelet-shaped particles and the spherical particles is given in Figure S4. The backscattering coefficient of two imaginary particles, spherical hBN and platelet $BaSO_4$, is also studied to systematically understand the respective roles of the refractive index and the particle morphology. The spherical hBN has a higher scattering coefficient than the platelet hBN; however, the platelet-shaped particle's lower asymmetry parameter results in a stronger backscattering coefficient in the ultraviolet, visible, and infrared wavelengths (Figure 3C), indicating that the platelet morphology is favorable than the spherical one, aside from refractive index. The results indicate that higher refractive index enhances the scattering coefficient, and the nanoplatelet morphology compromises the scattering coefficient slightly but overall enhances backscattering and eventually the backscattering coefficient, compared with $BaSO_4$ spherical nanoparticles.

As for the platelet orientations, the scattering coefficient (Figure 3D), asymmetry parameter (Figure 3E), and backscattering coefficient (Figure 3F) are studied for both the in-plane and cross-plane orientations, as well as a 45° angle between them. As expected, the angled orientation is overall lower in all values compared to the in-plane (horizontal) orientation and higher than the cross-plane (vertical) orientation.

Figure 3G shows the backscattering coefficient of hBN of various sizes (diameters of 100, 200, 400, and 800 nm with constant thickness of 50 nm). Once more, it is observed that each nanoplatelet diameter peaks the backscattering coefficient at distinct wavelength bands, implying the high variability in nanoparticle sizes can enhance the total reflectance.[18] Surprisingly, Rayleigh scattering-like asymmetry parameter is detected for hBN nanoplatelet at most of the regions including visible and infrared spectrum, regardless of size resulting in prominent backscattering. This is favorable for high solar reflectance.

The total reflectance of the four particles in Figures 3A–3C is also calculated by using the Monte Carlo method, and the results are shown in Figure 3H. The solar reflectance in the order from high to low are nanoplatelet hBN, spherical hBN, nanoplatelet $BaSO_4$, and spherical $BaSO_4$, indicating both high refractive index and nanoplatelet morphology favor high solar reflectance and explaining why hBN nanoplatelet-acrylic paints outperform $BaSO_4$-acrylic paints in solar reflectance. The simulated solar reflectance on the nanoplatelet hBN agrees with the experimental data reasonably well, as shown in Figure 2D. It is essential to mention the assumptions used to simplify the Monte Carlo model. No air pores were included in the nanocomposite as was observed from the SEM images, and nanocomposite consists of only single-size particles. These could result in an underprediction of total reflectance. On the other hand, our Monte Carlo method only uses scattering coefficient of light vertically incident on the hBN nanoplatelets, while no angular dependency is considered. This would cause overprediction of scattering and reflectance for an anisotropic material like hBN platelets. The agreement of the total solar reflectance between our experiment and Monte Carlo simulations, despite of capturing the main physics, can be due partly to error cancellation and hence should be interpreted with caution.

Cooling performance tests and analysis

The sky window emissivity for hBN-acrylic paints, at a value of 0.83, is relatively lower because of the lack of the sky window infrared-active phonon modes that contributes

Please cite this article in press as: Felicelli et al., Thin layer lightweight and ultrawhite hexagonal boron nitride nanoporous paints for daytime radiative cooling, Cell Reports Physical Science (2022), https://doi.org/10.1016/j.xcrp.2022.101058

to emissivity in $BaSO_4$-acrylic paints. However, during the daytime the sky window emissivity has much smaller role than the solar reflectance, and this is explained as follows. The overall radiative cooling capabilities of materials can be more fairly compared using the previously developed RC figure of merit[20], defined as

$$RC = \varepsilon_{sky} - r(1 - R_{solar}).$$

In this equation, ε_{sky} is the total sky window emissivity, r is the ratio of solar irradiation power over the blackbody surface emissive power in the sky window and is recommended to be set as ~7.14, assuming a standard 1,000 W/m^2 solar irradiation power and 140 W/m^2 blackbody surface emissive power in the sky window, and R_{solar} is the total solar reflectance. The physical meaning of RC is simple, that its multiplication with the blackbody surface emissive power in the sky window would yield the net radiative cooling power. From this definition, every 0.01 increment in the solar reflectance is equivalent to 0.0714 increment in the sky window emissivity in terms of the cooling performance. This figure of merit shows that cooling below ambient temperature can in principle be achieved when RC is positive. For an hBN-acrylic layer of 150 μm thickness, the RC is calculated at 0.68, demonstrating 68% radiative cooling capability over the theoretical limit. This is calculated from the 97.9% total solar reflectance measured for a 150 μm layer on a 1 mm glass substrate, and the 0.83 sky window emissivity calculated from measurements for a 150 μm layer on a 1 mm aluminum substrate. This can be compared with previous RC figures of merit for TiO_2-acrylic, $CaCO_3$-acrylic, $BaSO_4$ films, and $BaSO_4$-acrylic paint of 0.18, 0.62, 0.79, and 0.82, respectively.[21] It can also be compared with recent non-paintable approaches, which show RC values of 0.32,[8] 0.53,[10] 0.35,[9] and 0.57.[17] The RC for hBN-acrylic paints is among the highest calculated.

Furthermore, as a method to compare the performances of different materials while normalizing to layer thickness, a modified form of the originally given figure of merit is proposed:

$$RC_t = \left[\varepsilon_{sky} - r(1 - R_{solar})\right](1 - t/t_o),$$

where RC_t is the radiative cooling figure of merit with thickness taken into consideration, t is the layer thickness, and t_o is the maximum considered layer thickness (1 mm is recommended, as radiative cooling coatings are typically engineered to be below this thickness). This figure of merit is a rough approximation, and a truly accurate figure would likely involve a much more complicated expression. However, it can be used to roughly compare different materials. Using 1.5 mm for t_o, RC_t is calculated for various materials: 0.453 for $CaCO_3$-acrylic paints, 0.132 for TiO_2-acrylic paints, 0.701 for $BaSO_4$ films, 0.597 for $BaSO_4$-acrylic paints, and 0.612 for the studied hBN-acrylic paints.

Outdoor testing was performed to demonstrates the radiative cooling capability of the hBN-acrylic coatings. The test setup is shown in Figure 4A, and details are given in Experimental procedures. The ambient temperatures during outdoor tests vary between 20°C and 30°C, and the sample temperature is consistently lower than the ambient during daytime and nighttime (Figure 4B). Over the 3 days, an average temperature difference from the ambient was achieved of 6–8°C overall and 5–6°C during daylight hours (Figure 4C). Under the peak solar irradiation of 1,063 W/m^2, the sample can remain ~1–2°C cooler than the ambient because of the high solar reflectance. The total sky window emittance of 0.83 results in a maximum temperature difference of 12°C observed during the clear night on July 26, 2021. This experiment was further validated through comparison with a thermal balance model, described in detail in Note S1, Table S1, and Figure S5.

Please cite this article in press as: Felicelli et al., Thin layer lightweight and ultrawhite hexagonal boron nitride nanoporous paints for daytime radiative cooling, Cell Reports Physical Science (2022), https://doi.org/10.1016/j.xcrp.2022.101058

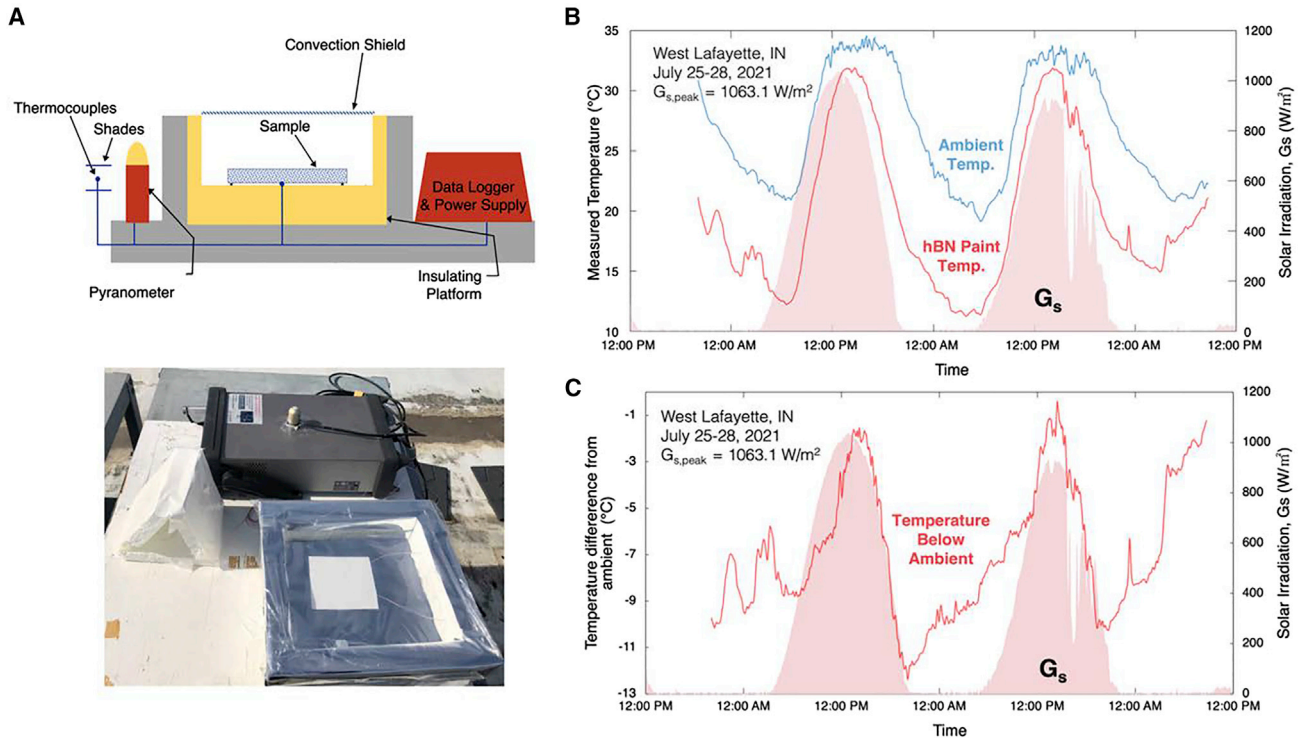

Figure 4. Field test setup and results

(A) Schematic and photo of the field test setup. Sample is placed in a Styrofoam insulating platform to reduce ground heating effects and 2 vertical and 1 horizontal transparent shield, made from thin polyethylene film are used around the sample to reduce forced convection loss. T-type thermocouples are used to collect temperature data of the bottom of sample, which is raised from the platform to avoid conduction loss, and the ambient, which is captured using a shaded thermocouple to avoid falsely high ambient temperature data from thermocouple overheating. The direct and diffuse solar irradiation is captured by the pyranometer.

(B) Temperature over time of the sample surface, as well as of the ambient surroundings, from outdoor experiments over three consecutive days from July 25–28, 2021. The measured average dew point for this period was 19.2 ± 1.2°C, and relative humidity was 72.9% ± 19.3%. The test was performed with samples with an average of 140-μm-thick 60% hBN-acrylic coatings on 1 mm aluminum sheets of approximately 2 × 2 inches. Samples were coated via pouring and checked for consistency in layer thickness at several points throughout the surface. Data demonstrate moving average over 10 min increments of the measured data.

(C) Temperature difference between the ambient surroundings and the sample surfaces. Data demonstrate moving average over 10 min increments of the measured data.

Reliability tests and viscosity characterization

A vital aspect of radiative cooling coatings is the feasibility of application, as well as the durability in outdoor use. Our 60% hBN-acrylic samples, made to 150 μm layer thickness on 1 mm aluminum sheet substrates, were subjected to several tests to demonstrate adequate performance in these regards. In Figure 5A, the samples are tested for mass-loss while undergoing 2,000 cycles of abrasion testing. Over this range, the mass loss experienced by the hBN-acrylic coating is comparable with that of commercial white paint and slightly outperforms previously developed calcite paints.[20] These results show that the wear of the developed coatings is similar to materials currently in use, and therefore demonstrate that the proposed material meets existing material performance in its resistance to mass loss from abrasion. Another aspect of concern in outdoor use is exposure to water. The hBN-acrylic coating samples were tested for water resistance by being submerged in circulating water for 24 h. The samples were weighed before the experiment, as well as after 24 h of drying time in the fume hood after the experiment. A net-zero mass loss was calculated, demonstrating good water resistance.[27]

Please cite this article in press as: Felicelli et al., Thin layer lightweight and ultrawhite hexagonal boron nitride nanoporous paints for daytime radiative cooling, Cell Reports Physical Science (2022), https://doi.org/10.1016/j.xcrp.2022.101058

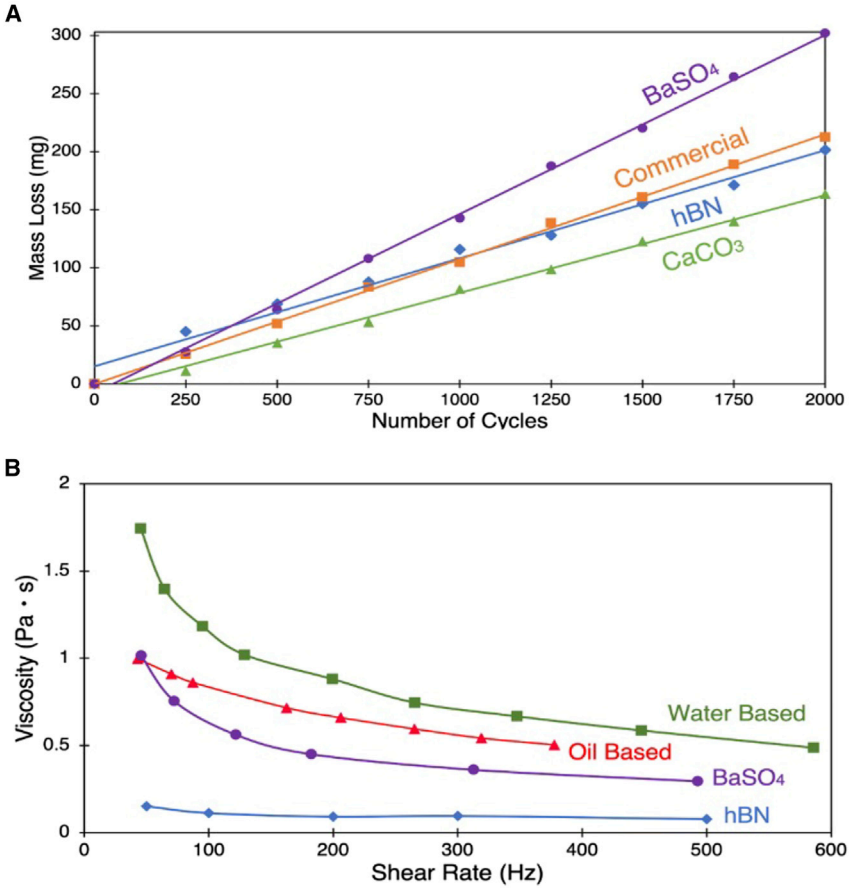

Figure 5. Results of abrasion and viscosity testing for 60% hBN-acrylic samples with a coating thickness of 150 μm on 1 mm aluminum sheet substrates

(A) Abrasion testing results for hBN paint (denoted as boron nitride) compared with commercial paints[19] and the previously developed calcite-based and barite-based paints.[20,21] Measurements of sample mass loss over 2,000 cycles are demonstrated.

(B) Viscosity testing for hBN (denoted as boron nitride) compared with commercial oil-based and water based paints[29] as well as the previously developed barite paint.[21] Measurements of the viscosity were performed at several shear rates from 10 to 600 s^{-1} for each sample.

To demonstrate ease and versatility of application techniques for the hBN-acrylic coatings, a viscosity test was carried out and result were compared with commercial paints[28] and the previously developed barite paint.[21] The viscosity was measured at constant sample temperature throughout and at various shear rates in the range of 50 and 500 s^{-1}. As illustrated in Figure 5B, the hBN-acrylic paint showed slight shear thinning, as well as a relatively lower viscosity compared with other paints. However, it remains within the industry recommended range of viscosities for brushing application of paints and coatings.[28]

Thinness, light weight, and their significant benefits

For easier comparison, Table 1, shows properties of various materials proposed in literature as well as those of the hBN-acrylic paints proposed in this work. Compared with the $BaSO_4$-acrylic paint that shows 98.1% solar reflectance,[21] the hBN-acrylic paint here shows 97.9% solar reflectance, but the thickness and weight are reduced by 62.5% and 78.4%, respectively. Even when compared with the porous polymers that show 96% solar reflectance,[17] our hBN-acrylic paint shows higher solar

Please cite this article in press as: Felicelli et al., Thin layer lightweight and ultrawhite hexagonal boron nitride nanoporous paints for daytime radiative cooling, Cell Reports Physical Science (2022), https://doi.org/10.1016/j.xcrp.2022.101058

Table 1. Summary and comparison of the proposed hBN-acrylic paint and previous radiative cooling materials in literature

Material type	Main component	Thickness, μm	Total density, g/cm^3	Weight, g/cm^2	Feature size, nm	total solar reflectance, %	sky window emissivity	RC_t
hBN-acrylic paint (proposed)	boron nitride (60% volume loading)	150	1.9	0.029	332	97.9	0.83	0.612
$BaSO_4$-acrylic paint[21]	barium sulfate (60% volume loading)	400	3.34	0.134	500	98.1	0.95	0.597
TiO_2-acrylic paint[20]	titanium oxide (8% volume loading)	400	3.18	0.127	100	89.5	0.93	0.132
$CaCO_3$-acrylic paint[20]	calcium carbonate (60% volume loading)	400	2.23	0.089	500	95.5	0.94	0.453
Porous polymeric coating[17]	poly(vinylidene fluoride-co-hexafluoropropylene)	300	1.77	0.053	200, 5,500	96	0.97	0.547
hBN photonic film[13]	boron nitride (40.5% volume loading)	1,400	–	–	900	98	0.89	0.05

reflectance while the thickness and weight are still reduced by 50% and 45.3%, respectively. It should be noted that the $BaSO_4$-acrylic paint[19,21] and $CaCO_3$-acrylic paint[19,20] were porous too, but their porosity is unknown at this time hence not counted in calculating their density, which would otherwise decrease to some extent. However, it remains clear that the hBN paint has the advantage in lowest thickness, lowest weight, and among the highest solar reflectance and quite high sky window emissivity, resulting in having the highest RC_t value among the compared materials.

It is noted that the cost of hBN nanoplatelets is higher than that of $BaSO_4$ nanoparticles. However, there is still significant benefit to a lightweight, thin paint layer of hBN in weight-sensitive applications requiring radiative cooling, such as aerospace technologies, airplanes, vehicles, and wearable technology. In wearables, typically only a small amount of lightweight coating is needed. In aircraft, seemingly small reductions in weight can result in significant decreases in fuel consumption and related CO_2 emissions. For example, we estimate that if the hBN-acrylic paint rather than $BaSO_4$-acrylic paint is used on all the 23,000 airplanes in operation globally, the total fuel savings would be 340,000 metric tons, and the CO_2 emission reduction would be ~1 million metric tons on a yearly basis. More details on this estimate can be found in Note S2.

In terms of the thickness, each coat by brush or roller only adds 50–75 μm of paint when dried, and more than 5–8 coats would be needed to reach 400 μm or mm-thick layers that have previously been needed. With the 150 μm hBN paint introduced in this work, the thickness of radiative cooling paints is brought to the common practical range, and only two coats are needed on average.

For the above reasons, the light weight and thinness are a significant innovation within this work. It provides a feasible option for a critical challenge of radiative cooling paints in many practical applications. The thin, lightweight, ultrawhite paint introduced in this work is expected to make a major impact in the field.

In this work, we have designed and fabricated a low-density, high-concentration nanoplatelet-based hBN-acrylic nanoporous paint and experimentally demonstrated their radiative cooling performance at low coating thickness, as defined by high solar reflectance and high sky window emissivity. At 150 μm thickness, the coating achieved a solar reflectance of 97.9% and a sky window emittance of 0.83. These are highly competitive values compared with others reported for greater coating thickness, and among coating and non-coating solutions for radiative cooling that have previously been developed. The weight is only 0.029 g/cm^2 because of

Please cite this article in press as: Felicelli et al., Thin layer lightweight and ultrawhite hexagonal boron nitride nanoporous paints for daytime radiative cooling, Cell Reports Physical Science (2022), https://doi.org/10.1016/j.xcrp.2022.101058

low density of the hBN nanoplatelets and the acrylic matrix, a porosity of 44.3%, and the thinness of the paint layer. The thickness and weight represent significant reductions from previous records for radiative cooling paints. Furthermore, this paint yields an average of 6–8°C cooling below ambient temperature. These results were due to the nanoplatelet morphology, moderately high electron bandgap of the hBN filler at 5.96 eV which eliminates UV absorption and yields higher refractive index, nanoporous nature, as well as the high concentration within the acrylic matrix at 60% volume loading. An average size in the neighborhood of peak solar wavelength and a broad size distribution also contribute to the high solar reflectance considerably. Abrasion, viscosity, and water resistance testing demonstrate that the paint is durable for outdoor use relative to other coatings and possesses a low viscosity that gives it a high degree of versatility when it comes to application techniques. The low density of the hBN nanoplatelets and the acrylic matrix, and the porosity of 44.3% help achieve a coating paint that is thin and lightweight. It could better enable practical applications such as on buildings and automobiles, and lightweight applications such as on aircraft and fabrics.

EXPERIMENTAL PROCEDURES

Resource availability

Lead contact

X.R. is the lead contact; email address: ruan@purdue.edu.

Materials availability

hBN-acrylic paints generated in this study may be made available on request.

Data and code availability

All data and original codes mentioned in this study will be made available upon request from the research community.

hBN nanoplatelet-acrylic paint sample fabrication

PCTP2 hBN nanoplatelets were acquired from Saint Gobain Advanced Ceramics, LLC and added in small quantities to DMF while stirring until all hBN was incorporated. The DMF solvent was used to lower viscosity of the material. The mixture was sonicated for 5 min to ensure uniform nanoplatelet distribution. Elvacite 2028 acrylic powder from Lucite International, the chosen matrix material for its low viscosity, was then gradually added to the mixture while stirring until dissolved fully. The overall solid/liquid ratio is 1:6. To help with the high viscosity of the material, the stir plate was used to heat it slightly to 30°C. This final mixture was sonicated once again for 10 min to ensure uniformity. Samples were poured in even layers onto 1-mm-thick glass slides or 1 mm aluminum plates and left in a hood for a minimum of 6 h to allow the DMF solvent to fully evaporate. The thickness of the samples was measured at several locations using a caliper and/or profilometer.

Porosity calculation

The porosity of the final, dry material is calculated as

$$\%\ Porosity = \left(1 - \frac{Solid\ Sample\ Volume}{Total\ Sample\ Volume}\right) * 100.$$

Three samples were measured to determine the sample mass and calculate the solid sample volume. The samples were made by pouring the paint to fully cover 50 × 75 mm glass slide substrates with a consistent layer. The total sample volume for each sample was calculated by measuring the thickness of the poured layer once dry and multiplying by the area of the glass slide. The solid density was calculated

Please cite this article in press as: Felicelli et al., Thin layer lightweight and ultrawhite hexagonal boron nitride nanoporous paints for daytime radiative cooling, Cell Reports Physical Science (2022), https://doi.org/10.1016/j.xcrp.2022.101058

using the known density of the acrylic binder, 1.185 g/cm^3, and the hBN nanoplatelets, 2.1 g/cm^3, as well as the known volume ratio of acrylic/hBN of 4:6. Finally, the measured sample mass and solid density is used to calculate the solid sample volume after measuring the total mass of each sample and subtracting the mass of the glass slide substrate. Using these values, the average porosity of a dried paint layer is calculated to be 44.3%, with an SD of 1.4%.

Estimate of backscattering coefficient

Mie theory is an analytical solution and is widely used for the calculation of the scattering of a plane electromagnetic wave by homogeneous spherical particles and infinite cylinders. A different method is needed for a better approximation of the scattering coefficient and the asymmetry parameter of platelet particles, such as hBN nanoplatelets. In this work, we solve Maxwell's equation by using finite element method (FEM) and COMSOL Multiphysics.

For a homogeneous and linear medium, the electric field ($\boldsymbol{E}$) in the frequency domain is given as

$$\nabla \times (\nabla \times \boldsymbol{E}) - k_0^2 \epsilon_r \boldsymbol{E} = 0,$$

where k_0 is the wavenumber in free space, and ϵ_r is the relative permittivity. The light wave is mathematical approximated by a plane wave with the boundary condition

$$\boldsymbol{n} \times [\nabla \times (\boldsymbol{E} + \boldsymbol{E}_b)] - jk\, \boldsymbol{n} \times (\boldsymbol{E} \times \boldsymbol{n}) = 0,$$

where k is the wavenumber $\boldsymbol{E}_b$ is the scattered field defined as $\boldsymbol{E}_b = E_0 \exp\left(-\frac{2\pi j z}{\lambda}\right)\hat{\boldsymbol{x}}$, E_0 is the electric field magnitude, and λ is the wavelength.

The cross-section scattering (σ_{sc}) and the asymmetry parameter (g) are defined as

$$\sigma_{sc} = \frac{\int\int_S \boldsymbol{n} \cdot \boldsymbol{P}\, dS}{S_{in}} \text{ and } g = \frac{\int\int_S \cos\theta (\boldsymbol{n} \cdot \boldsymbol{P})\, dS}{\int\int_S \boldsymbol{n} \cdot \boldsymbol{P}\, dS},$$

where $\boldsymbol{P}$ is the power flow, $S_{in} = \frac{E_0^2}{2Z_0}$, Z_0 is the impedance of free space, and $\cos\theta = \boldsymbol{n} \cdot \boldsymbol{k}$. From these values, the total and backward scattering coefficients can be estimated.[29] Validation of this model is included in Figure S2.

Spectral characterization

The optical properties of the samples were characterized in both the UV-Vis-NIR and IR wavelengths using spectrometers. For the UV-Vis-NIR characterization, a PerkinElmer Lambda 950 spectrometer with an integrating sphere was used along with a Spectralon diffuse reflectance standard. The characterization in the IR wavelengths was performed on a Nicolet iS50 FTIR spectrometer with a PIKE integrating sphere and a PIKE Technologies diffuse reflectance standard. A 1-mm-thick glass plate substrate was used for the UV-Vis-NIR measurements to prevent contribution of the substrate to reflectance, and a 1-mm-thick aluminum sheet substrate was used for the IR measurements to avoid contribution of the substrate to emissivity. Although a freestanding sample or IR-transparent substrate is preferred for sky window emissivity measurements, this was not successfully attained at this point yet and will be attempted in the future. The spectral reflectance R_λ and transmittance T_λ from 0.25–20 μm were measured and quantified, and the spectral absorptance A_λ was calculated from measured values by $A_\lambda = 1 - R_\lambda - T_\lambda$. The sky window emissivity was calculated by first obtaining the absorptance at each wavelength from the measured reflectance and transmittance values, and then finding the total absorptance within the sky window, pertaining to 8–13 μm wavelengths.

Field test of radiative cooling performance

The radiative cooling performance of the samples is characterized by simultaneously monitoring sample temperature, ambient temperature, and solar irradiation. The outdoor experiment was conducted at West Lafayette, Indiana (40.4237°N, 86.9212°W) between July 25 and July 28, 2021. Figure 4A demonstrates the outdoor cooling setup. T-type thermocouples were attached to the back of the samples and suspended underneath the table to monitor the sample and ambient temperatures. The samples were placed in an insulating Styrofoam box and covered by a 12 μm PE film to mitigate conduction and convection loss without blocking the radiative heat exchange. The ambient temperature was used to calculate cooling below ambient temperature, as using air temperature in the sample compartment would overestimate the cooling capacity and weather station temperature would underestimate it. The solar irradiation is monitored by a pyranometer. The data collection occurred every minute and a moving average of 10 min intervals is plotted.

Durability characterization

The durability properties of the samples were characterized to represent various conditions representative of real-world use and application. Abrasion tests were conducted using a Taber Abraser Research Model and performed following ASTM D4060 guidelines.[30] Two CS-10 abrasive wheels with a loading of 250 g per wheel were placed on the surface of a 150-μm-thick layer of coating on a 1 mm flat aluminum sheet. The samples were weighed prior to testing, and reweighed every 250 cycles to quantify mass loss. According to the ASTM D4060 standard, the wheels were also resurfaced every 500 cycles for consistency. Mass loss was measured over a total 2,000 cycles. Overall wear was compared with coatings commonly used in similar applications.

In order to characterize the usability for various application techniques, the viscosity of the 60% hBN-acrylic coating was also measured across using a RheoSense microviscometer. At a consistent sample temperature of 23°C, the viscosity of a 50 μl sample of coating was measured across 5 discrete shear rates over a range of 50–500 s^{-1}. The results were compared with coatings commonly used in similar applications.

The potential effects of rain and other water exposure were also considered by following water resistance testing of coatings techniques as described in ASTM D870.[27] A 2 × 2 inch, 1-mm-thick flat aluminum sheet was coated with 150 μm of hBN-acrylic paint. The sample was then held in place fully submerged in a large container of gently circulating water (stirred at 280 rpm) with no contact with container walls. This setup was left in place for 24 h, with mass of sample being measured before testing. The mass was once again measured after allowing sample to dry for 24 h in a fume hood and the net mass loss was calculated.

SUPPLEMENTAL INFORMATION

Supplemental information can be found online at https://doi.org/10.1016/j.xcrp.2022.101058.

ACKNOWLEDGMENTS

We thank Jennifer Cahillane and Richard Smith at Purdue University for their assistance with sample fabrication, characterization, and measurements. The authors also thank Saint Gobain Advanced Ceramics LLC for donating the hBN materials. A.F. acknowledges support from the US National Science Foundation through a

Graduate Research Fellowship. I.K., Y.Z., and X.R. acknowledge partial support from the US National Science Foundation through award 2102645.

AUTHOR CONTRIBUTIONS

Conceptualization, X.R. and G.C.; Methodology, X.R., G.C., A.F., I.K., Y.Z., F.B., and Z.G.; Investigation, A.F., I.K., F.B., Y.Z., Z.G., and J.P.; Writing – Original Draft, A.F.; Writing – Review & Editing, X.R., G.C., A.F., I.K., F.B., Y.Z., Z.G., and J.P.; Resources, X.R. and G.C.; Supervision, X.R. and G.C. The manuscript was written through contributions from all authors. All authors have given approval to the final version of the manuscript.

DECLARATION OF INTERESTS

X.R., G.C., A.F., and I.K. are inventors of a provisional patent based on this work filed with the U.S. Patent and Trademark Office on August 28, 2021. The application number is 63238124.

INCLUSION AND DIVERSITY

One or more of the authors of this paper self-identifies as an underrepresented ethnic minority in their field of research or within their geographical location. One or more of the authors of this paper self-identifies as a gender minority in their field of research. One or more of the authors of this paper received support from a program designed to increase minority representation in their field of research.

Received: September 27, 2021
Revised: July 12, 2022
Accepted: August 30, 2022
Published: October 3, 2022

REFERENCES

1. US Department of Energy (2022). Air Conditioning. https://www.energy.gov/energysaver/air-conditioning.

2. Barker, R. (1875). The process of making ice in the east-indies. Sci. Am. *13*, 75. https://doi.org/10.1098/rstl.1775.0023.

3. Munday, J.N. (2019). Tackling climate change through radiative cooling. Joule *3*, 2057–2060. https://doi.org/10.1016/j.joule.2019.07.010.

4. Harrison, A.W., and Walton, M.R. (1978). Radiative cooling of TiO_2 white paint. Sol. Energy *20*, 185–188. https://doi.org/10.1016/0038-092x(78)90195-0.

5. Orel, B., Gunde, M., and Krainer, A. (1993). Radiative cooling efficiency of white pigmented paints. Sol. Energy *50*, 477–482. https://doi.org/10.1016/0038-092x(93)90108-z.

6. Pockett, J. (2010). Heat reflecting paints and a review of their advertising material. In Chemeca 2010: Engineering at the Edge (Hilton Adelaide), pp. 1–13.

7. Holynska, M., Butenko, Y., Martins, R., Semprimoschnig, C., Meyer, F., and Faber, S. (2019). Studies of white ceramic coatings for ESA's BepiColombo mission to mercury. J. Spacecraft Rockets *56*, 1358–1370. https://doi.org/10.2514/1.a34230.

8. Raman, A.P., Anoma, M.A., Zhu, L., Rephaeli, E., and Fan, S. (2014). Passive radiative cooling below ambient air temperature under direct sunlight. Nature *515*, 540–544. https://doi.org/10.1038/nature13883.

9. Kou, J.l., Jurado, Z., Chen, Z., Fan, S., and Minnich, A.J. (2017). Daytime radiative cooling using near-black infrared emitters. ACS Photonics *4*, 626–630. https://doi.org/10.1021/acsphotonics.6b00991.

10. Zhai, Y., Ma, Y., David, S.N., Zhao, D., Lou, R., Tan, G., Yang, R., and Yin, X. (2017). Scalable-manufactured randomized glass-polymer hybrid metamaterial for daytime radiative cooling. Science *355*, 1062–1066. https://doi.org/10.1126/science.aai7899.

11. Li, T., Zhai, Y., He, S., Gan, W., Wei, Z., Heidarinejad, M., Dalgo, D., Mi, R., Zhao, X., Song, J., et al. (2019). A radiative cooling structural material. Science *364*, 760–763. https://doi.org/10.1126/science.aau9101.

12. Yang, Z., Zhou, Z., Sun, H., Chen, T., and Zhang, J. (2021). Construction of a ternary channel efficient passive cooling composites with solar-reflective, thermoemissive, and thermoconductive properties. Compos. Sci. Technol. *207*, 108743. https://doi.org/10.1016/j.compscitech.2021.108743.

13. Li, P., Wang, A., Fan, J., Kang, Q., Jiang, P., Bao, H., and Huang, X. (2021). Thermo-optically designed scalable photonic films with high thermal conductivity for subambient and above-ambient radiative cooling. Adv. Funct. Mater. *32*, 2109542. https://doi.org/10.1002/adfm.202109542.

14. Rephaeli, E., Raman, A., and Fan, S. (2013). Ultrabroadband photonic structures to achieve high-performance daytime radiative cooling. Nano Lett. *13*, 1457–1461. https://doi.org/10.1021/nl4004283.

15. Huang, Z., and Ruan, X. (2017). Nanoparticle embedded double-layer coating for daytime radiative cooling. Int. J. Heat Mass Tran. *104*, 890–896. https://doi.org/10.1016/j.ijheatmasstransfer.2016.08.009.

16. Atiganyanun, S., Plumley, J.B., Han, S.J., Hsu, K., Cytrynbaum, J., Peng, T.L., Han, S.M., and Han, S.E. (2018). Effective radiative cooling by paint-format microsphere-based photonic random media. ACS Photonics *5*, 1181–1187. https://doi.org/10.1021/acsphotonics.7b01492.

17. Mandal, J., Fu, Y., Overvig, A.C., Jia, M., Sun, K., Shi, N.N., Zhou, H., Xiao, X., Yu, N., and Yang, Y. (2018). Hierarchically porous polymer coatings for highly efficient passive daytime radiative cooling. Science *362*, 315–319. https://doi.org/10.1126/science.aat9513.

18. Peoples, J., Li, X., Lv, Y., Qiu, J., Huang, Z., and Ruan, X. (2019). A strategy of hierarchical

particle sizes in nanoparticle composite for enhancing solar reflection. Int. J. Heat Mass Tran. *131*, 487–494. https://doi.org/10.1016/j.ijheatmasstransfer.2018.11.059.

19. Ruan, X., Peoples, J., Li, X., and Huang, Z. (2020). Metal-free solar-reflective infrared-emissive paints and methods of producing the same. US Patent and Trademark Office, International Application No. PCT/US2019/054566.

20. Li, X., Peoples, J., Huang, Z., Zhao, Z., Qiu, J., and Ruan, X. (2020). Full daytime sub-ambient radiative cooling with high figure of merit in commercial-like paints. SSRN J. https://doi.org/10.2139/ssrn.3652325.

21. Li, X., Peoples, J., Yao, P., and Ruan, X. (2021). Ultrawhite BaSO4 paints and films for remarkable daytime subambient radiative cooling. ACS Appl. Mater. Interfaces *13*, 21733–21739. https://doi.org/10.1021/acsami.1c02368.

22. Mandal, J., Yang, Y., Yu, N., and Raman, A.P. (2020). Paints as a scalable and effective radiative cooling technology for buildings. Joule *4*, 1350–1356. https://doi.org/10.1016/j.joule.2020.04.010.

23. Tong, Z., Peoples, J., Li, X., Yang, X., Bao, H., and Ruan, X. (2022). Electronic and phononic origins of BaSO4 as an ultra-efficient radiative cooling paint pigment. Materials Today Physics *24*, 100658. https://doi.org/10.1016/j.mtphys.2022.100658.

24. McKay, M.A., Li, J., Lin, J.Y., and Jiang, H.X. (2020). Anisotropic index of refraction and structural properties of hexagonal boron nitride epilayers probed by spectroscopic ellipsometry. J. Appl. Phys. *127*, 053103. https://doi.org/10.1063/1.5134908.

25. Lee, S., Jeong, T., Jung, S., and Yee, K. (2018). Refractive index dispersion of hexagonal boron nitride in the visible and near-infrared. Phys. Status Solidi B *256*, 1800417. https://doi.org/10.1002/pssb.201800417.

26. Golla, D., Chattrakun, K., Watanabe, K., Taniguchi, T., LeRoy, B.J., and Sandhu, A. (2013). Optical thickness determination of hexagonal boron nitride flakes. Appl. Phys. Lett. *102*, 161906. https://doi.org/10.1063/1.4803041.

27. ASTM Subcommittee D0127. (2020). Standard Practice for Testing Water Resistance of Coatings Using Water Immersion, *6.01* (ASTM Book of Standards).

28. Whittingstall, P. (2011). Paint evaluation using rheology. TA Instruments Thermal Analysis and Rheology. RH 059.

29. Bohren, C.F., and Huffman, D.R. (1998). Absorption and Scattering of Light by Small Particles (Wiley), pp. 82–157.

30. ASTM Subcommittee D01.23 (2010). Standard Test Method for Abrasion Resistance of Organic Coatings by the Taber Abraser, *6.01* (ASTM Book of Standards).

Cell Reports Physical Science, Volume *3*

Supplemental information

Thin layer lightweight and ultrawhite hexagonal boron nitride nanoporous paints for daytime radiative cooling

Andrea Felicelli, Ioanna Katsamba, Fernando Barrios, Yun Zhang, Ziqi Guo, Joseph Peoples, George Chiu, and Xiulin Ruan

Supplementary Material

Thin Layer Lightweight and Ultrawhite Hexagonal Boron Nitride Nanoporous Paints for Daytime Radiative Cooling

Felicelli *et al.*

Supplementary Text

Note S1: Thermal Balance Model.

For confirmation of experimental results from the outdoor radiative cooling experiments, a theoretical thermal balance was done using finite difference methods. The change in temperature over time was estimated using the following expression:

$$\left(m_p c_{pp} + m_s c_{ps}\right)\frac{dT}{dt} = h(T_a - T) - P_{rc}$$

Where T is the paint sample temperature, t is time, T_a is ambient temperature, and P_{rc} is cooling power. Other constants are listed and quantified in Table S1.

Table S1. Constants for Thermal Balance Model

Constant	Value
Specific heat of Paint, C_{pp} (J/kgK)	1054.4
Specific heat of Substrate, C_{ps} (J/kgK)	910
Mass of Paint for area, m_p (kg/m^2)	0.26
Mass of Substrate for area, m_s (kg/m^2)	2.7
Time step, dt (s)	60

Convection Coefficient, h (W/m^{2}K)	8
Total Solar Reflection, r	0.979
Sky Window Emissivity, ε_{sw}	0.83
Sky Window Band Fraction, F_{sw}	0.313
Emissivity Outside Sky Window, ε_n	0.71

Ambient temperature, solar irradiation, relative humidity, and actual sample temperature values were acquired from measurements during outdoor experiments. The cooling power was calculated using the following expression:

$$P_{rc} = P_{rad} - \alpha P_{sun}$$

Where P_{rad} is the radiation loss, α is solar absorption of the sample, and P_{sun} is solar irradiation. The radiation loss, P_{rad}, is calculated using:

$$P_{rad} = -\sigma[\varepsilon_n(T_a^4 - T^4)(1 - F_{sw}) - e_{sw}T^4c]$$

Where σ is the Stefan-Boltzmann constant, and c is the humidity effects in the sky window as described by A.W. Harrison.[1]

The results of the model are plotted against the experimental results below. The error between the model and experiments was calculated to be 8.2 ± 2.9%. Our model demonstrates excellent agreement with the experimental results.

Note S2: Fuel Consumption and CO_2 Emissions in Aircraft.

It has been estimated that for 1 kg of weight reduction in an aircraft, 74 kg fuel can be saved on average per year.[2] Furthermore, it is known that for aircraft, every 1 kg of fuel used (regardless of flight phase), 3.16 kg of CO_2 is emitted.[3] It can therefore be estimated that for just 1 kg weight saving on aircraft, the CO_2 emissions are reduced by 233.8 kg per year. Seeing as the paint of an

aircraft can add between 273-544 kg of extra weight,[4] it becomes clear that lightweight, low thickness paints can significantly contribute to reducing fuel consumption and CO_2 emissions. Take a conservative assumption that using our hBN paint could save 200 kg weight for an aircraft compared to the $BaSO_4$ paint, and consider there are ~23,000 airplanes in operation globally, we can estimate that the total fuel savings would be 340,000 metric tons and the CO_2 emission reduction would be ~ 1 million metric tons on a yearly basis. This is before considering the benefits of radiative cooling, which further reduces these quantities due to less energy usage needed for space cooling on aircraft, which is particularly needed to keep aircraft cool when spending many hours in direct sunlight at airports between flights.

Supplementary Figures:

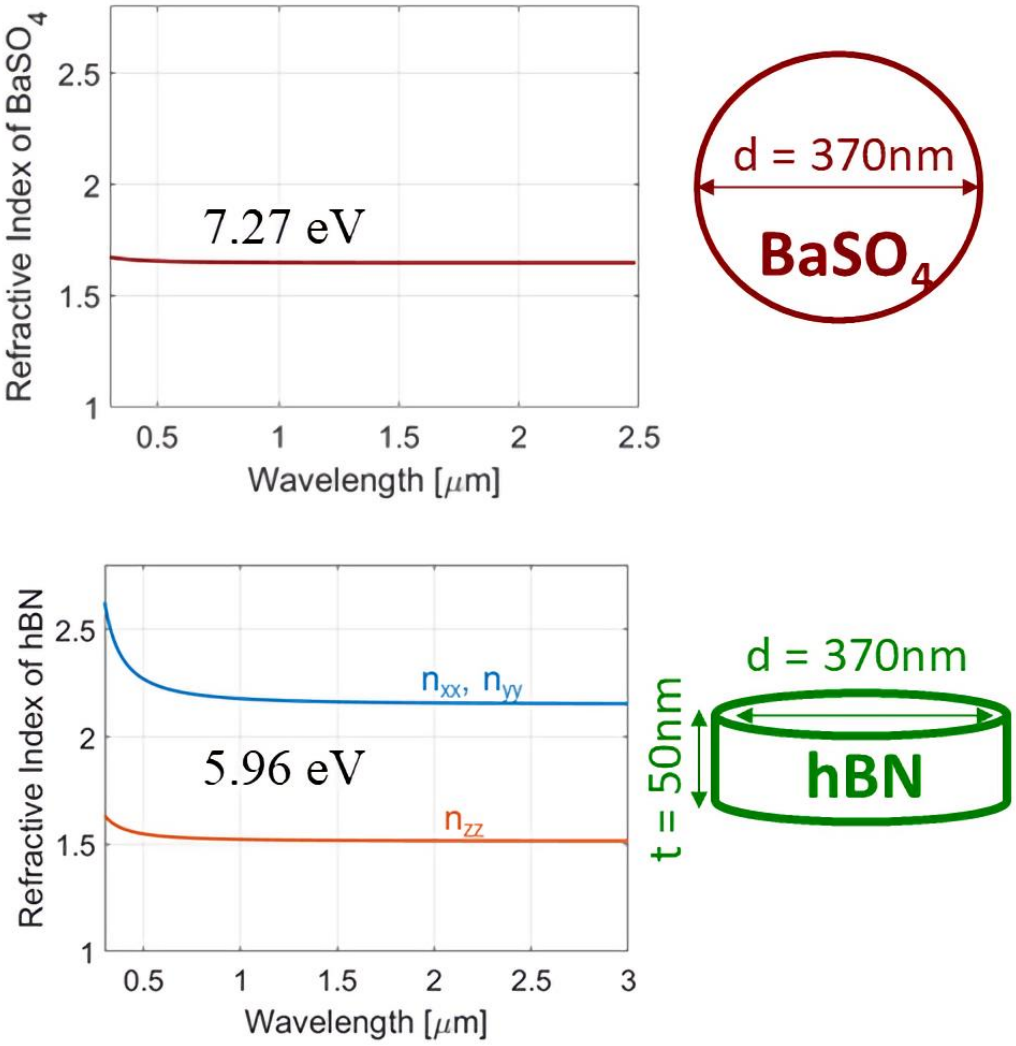

Figure S1. Refractive index of BaSO4 (on top) and hBN (on bottom). Hexagonal BN has a higher refractive index due to a smaller bandgap of 5.96eV than BaSO4 bandgap of 7.27eV. In addition, hBN has a platelet morphology resulting in anisotropic properties with different in-plane (parallel to the electric field) and out-of-plane (vertical to the electric field) refractive indices.

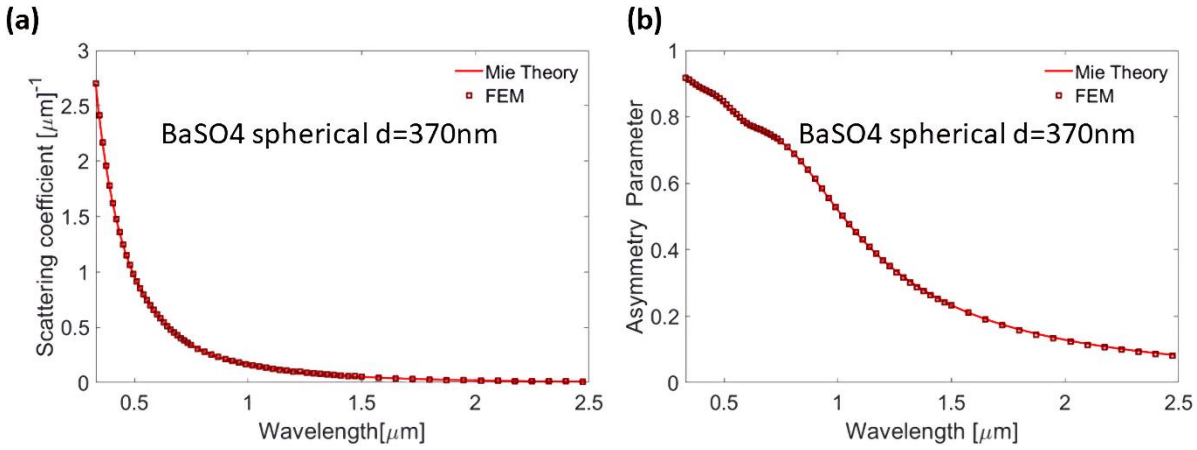

Figure S2. Validation of the FEM against the Mie theory. Results from Mie Theory model for spherical $BaSO_4$ nanoparticles are compared to the results from the FEM model for the same diameter (d = 370nm). There is good agreement between models, indicating accuracy of the FEM code used. **(a)** Scattering coefficient and **(b)** Asymmetry parameter of spherical $BaSO_4$.

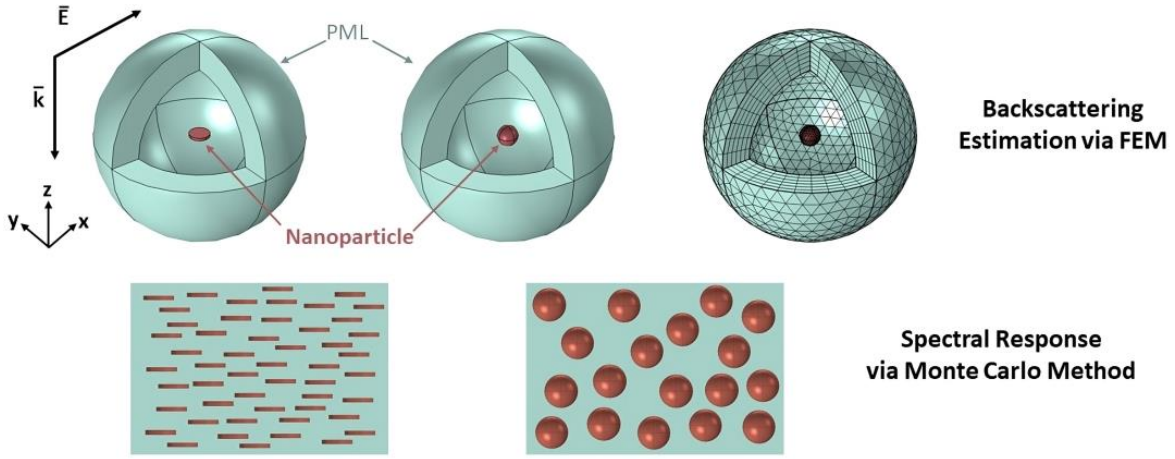

Figure S3. Schematic of the computational methods. For the calculation of the backscattering of a single particle with spherical and platelet shapes, FEM was used. Then the backscattering was used as an input in the Monte Carlo method to estimate the spectral response of nanocomposites with particle volume fraction of 60%.

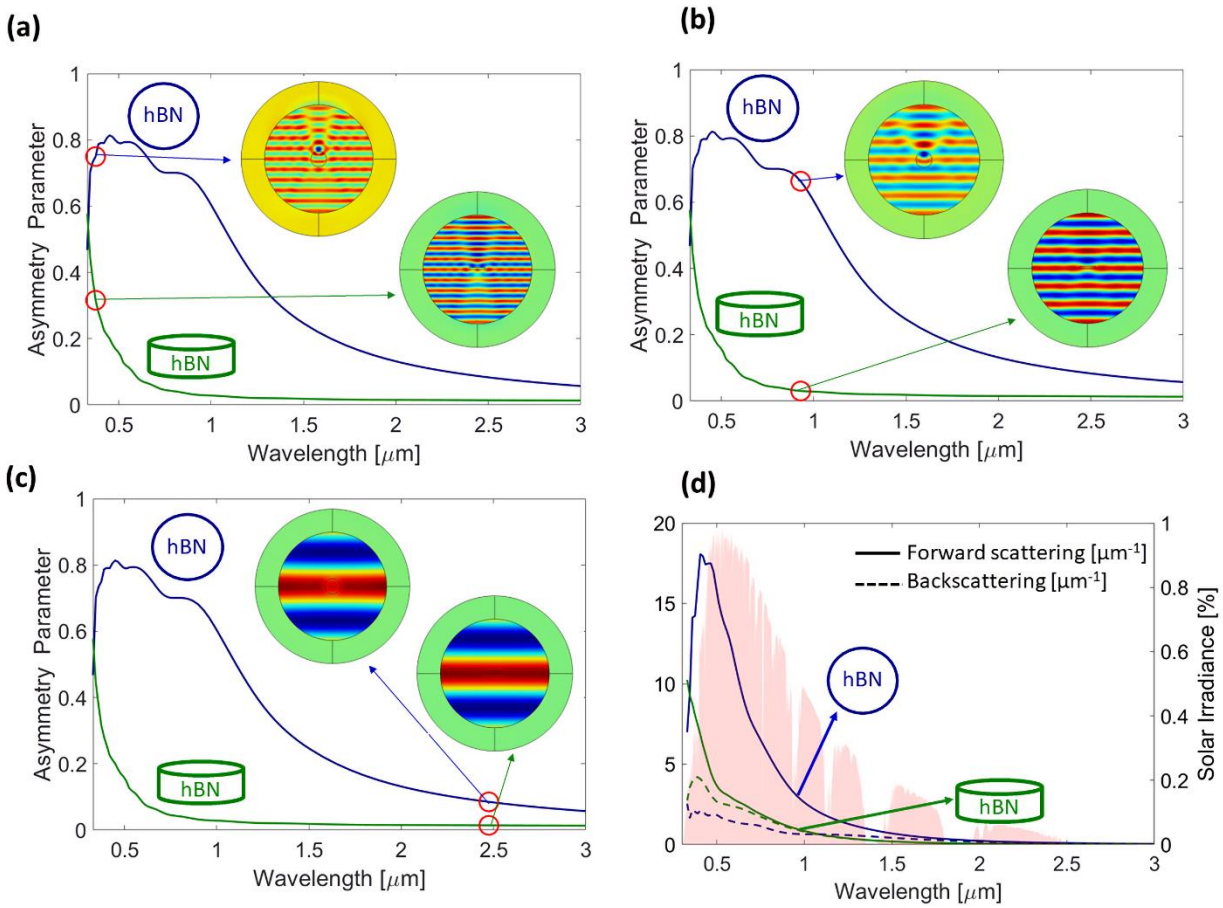

Figure S4. The effect of morphology on the asymmetry parameter. We compare the two particles (hBN sphere and hBN platelet) with the same refractive index but different shapes. **(a)** Asymmetry parameter at wavelength of 250 nm. The spherical particle has geometric scattering in contrast with the platelet particle, which behaves more like Mie scattering. **(b)** Asymmetry parameter at wavelength of 420 nm. The spherical particle has Mie scattering, and the platelet particle starts to behave like Rayleigh scattering **(c)** Asymmetry parameter at wavelength of 1650 nm. Both particles have Rayleigh scattering. **(d)** Forward- and back-scattering coefficients of the two particles.

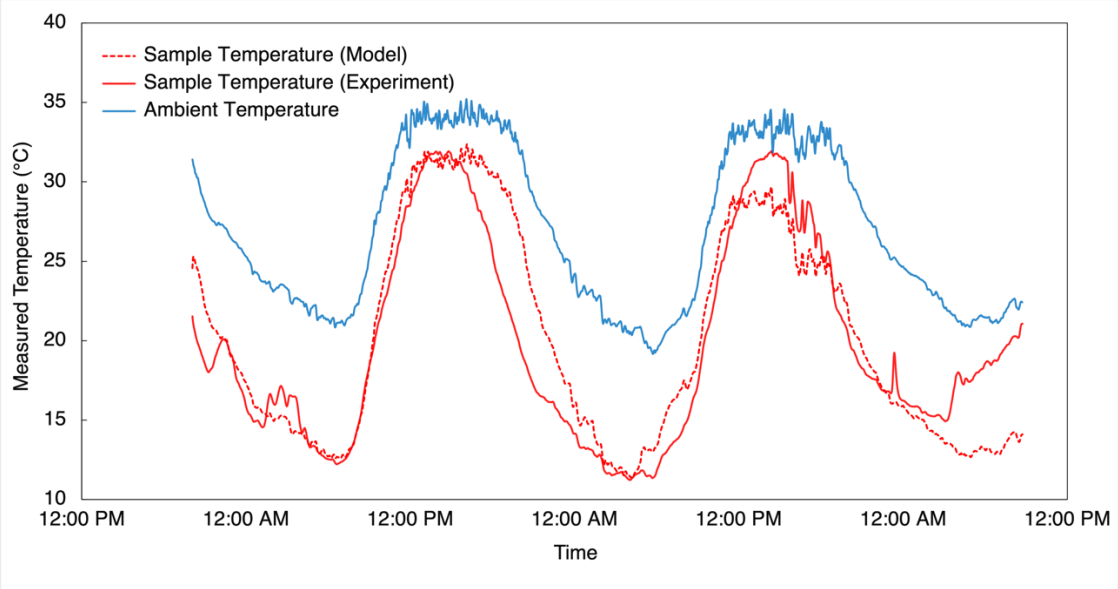

Figure S5. Plot of thermal model results versus experimental results, demonstrating sample temperature difference the from measured ambient temperature.

Supplementary References

1. Harrison, A.W. (1981). Effect of Atmospheric Humidity on Radiation Cooling. Solar Energy. vol. 26, pp 243-247.
2. Gilani, M., Körpe, D. (2019). Airline Weight Reduction to Minimize Direct Operating Cost. Intavic - The 4th International Aviation Management.
3. Skowron, A., Lee, D.S., De León, R.R., Lim, L.L. and Owen, B. (2021). Greater fuel efficiency is potentially preferable to reducing NOx emissions for aviation's climate impacts. Nature Communications, 12(1). doi:10.1038/s41467-020-20771-3.
4. Hansen, D. (1999). Painting versus Polishing of Airplane Exterior Surfaces. Boeing Aero Magazine, vol. 5.